IMPLOSION-DRIVEN SHOCK TUBE

I. I. GLASS   J. C. POINSSOT
Institute for Aerospace Studies
University of Toronto   N G-R-52-026-023

SUMMARY

Stoichiometric mixtures of hydrogen-oxygen at 200, 400, and 600
psi initial were detonated at the geometric centre of an 8 in dia
hemispherical chamber by a very short exploding wire. The deton-
ation wave in the mixture moves out towards the periphery where it
can strike a shell of PETN explosive to produce an explosive-driven
implosion or it may be allowed to reflect from the steel surface only,
without an explosive liner, as an implosion wave moving into a highly
preheated gas. As expected, for the gas runs only, the shock strength
increases nonlinearly with initial pressure. For 600 psi initial, a
shock Mach number, $M_S=40$, was obtained in a 8 mm dia channel
filled with air at 1 torr. The shock decayed to $M_S=11$, over about
~180 cm. Blast-wave decay, and viscous and ablative losses un-
doubtedly cause the high attenuation. A numerical analysis predicts
shock Mach numbers $M_S \sim 100$, using a modest loading of 200 g
PETN and 200 psi $2H_2 + O_2$. The small barrel bore was used to check
out the limiting case when the facility is used as a massles-projectile
hypervelocity launcher or shock tube. Explosive runs will be made
in 8 mm and 25 mm dia channels, using the 8 in dia driver chamber,
in the near future.

1. INTRODUCTION

The controlled generation of strong, symmetrical implosion waves
in a reusable facility by using safe, secondary explosives is described
in Ref 1. Basically (see Fig 1), an 8 in dia hemispherical chamber
is filled with a mixture of $2H_2 + O_2$ to several hundred psi. The mix-
ture is detonated by a short exploding copper wire (1/16 in long x
0.002 in dia), as shown in Fig 1A. The detonation wave races at
about 2.9 km / sec to impact on a hemispherical shell of PETN
weighing several hundred grams (2 to 6 mm thick), in order to

detonate it impulsively and simultaneously, and send an implosion wave into the highly preheated gas (about 3,000° K) to further heat and compress it as it collapses and reflects at the origin, (see Fig 1B).

The pocket of gas at the origin can be used as a driver for a hyper-velocity launcher or a shock tube, (see Fig 1C), or for many other physical experiments requiring such a pocket of concentrated high-pressure, high-temperature gas.[2, 3, 4] Implosions produced in this manner have been used to drive plastic projectiles (7.9 mm dia x 7.9 mm long, that is, 5/16 in dia single-calibre cylinders), weighing 356 mg, to velocities up to 17,600 ft/sec. Although numerical analyses showed that velocities which are factors greater than the above should ideally have been achieved, it was concluded that prob-lems of projectile integrity and those arising from viscous and ablative losses would limit the actual velocities which could be obtained.

The numerical analyses[5, 6, 7] consist of solving the set of nonlinear partial differential equations of mass, momentum and energy in Lagrangian form, with the aid of equations of state. The set of equations is solved by numerically integrating a set of corresponding finite difference equations, using an artificial viscosity technique, subject to prescribed initial and boundary conditions[8, 9, 10, 11] for hypervelocity launchers and shock tubes.

It is important to note that the shock tube can be considered as a special case of the hypervelocity launcher, where the projectile mass is reduced to zero, or the case of the massless projectile. In view, of the actual loss mechanisms that exist to limit projectile velocity, it was considered very worthwhile examining the massless projectile case, since it does not suffer from projectile disintegration, friction, ablation, and leakage problems.[1]

2. NUMERICAL ANALYSIS

Both, the hypervelocity launcher and the shock tube have been studied analytically, as noted above. The numerical analysis con-sists of solving the set of lossless (no friction, heat transfer or ablation) nonlinear partial differential equations of mass, momentum and energy, in Lagrangian form, with the aid of the equations of state, as follows[5, 6]:

mass:
$$V = \frac{1}{\rho} = \frac{1}{\delta} \frac{\partial R^{\delta}}{\partial m} \tag{1}$$

momentum:
$$\frac{\partial U}{\partial t} = -A \frac{\partial (P + Q)}{\partial m} \tag{2}$$

$$\text{energy:} \qquad \frac{\partial E}{\partial t} = -(P+Q)\frac{\partial V}{\partial t} \qquad (3)$$

$$\text{state:} \qquad E = E(P, V), \qquad (4a)$$

for gas mixtures $2H_2 + O_2$
and air

$$P = P(E, V), \qquad (4b)$$

for the explosive, PETN.

The artificial-viscosity pressure[7], Q, is restricted to compression waves only, and is expressed as

$$Q = \frac{(C \Delta x)^2}{V} \cdot \left(\frac{\partial U}{\partial x}\right)^2 \qquad (5a)$$

$$\text{for} \quad \frac{\partial U}{\partial x} < 0$$

$$\text{and } Q = 0 \qquad (5b)$$

$$\text{for} \quad \frac{\partial U}{\partial x} \gtrless 0$$

where, A = area of elemental interface
C = artificial viscosity constant
$m = \frac{1}{\delta} \rho_0 R_0^{\delta}$, mass per stearadian

δ = 1, 2, 3 for planar, cylindrical, and spherical geometries, respectively

ρ_0 = initial density
R_0 = initial position of Lagrangian surface
U = particle velocity
V = specific volume
R = radial distance .
P = pressure
Q = artificial viscosity pressure
E = specific interval energy
t = time
Δx = zone width in difference scheme

The system is divided into three regions (see Fig 2): the explosive PETN, the gas mixture $2H_2 + O_2$, and the air in the channel. Each has its own equation of state. Each region is divided into zones, and mass points contaning one half of the mass of two adjacent zones

are assumed to be at the interface of these zones.

Equations 1 to 5 are then solved by numerically integrating a set of corresponding finite difference equations, using the artificial viscosity technique subject to the prescribed initial and boundary conditions.[8, 9, 10, 11] Using the artificial viscosity, which spreads the shock over a specified number of zones, avoids treating the shock wave discontinuities running through discrete mass points by spreading them over about 3 to 6 zones.

The two independent variables time and distance are represented by the number of the cycle, N, in the computational scheme which is being calculated, and J, the label assigned to a mass point (Fig 2). The finite difference equations can be written as follows:

mass:
$$V_{J-1/2}^{N} = \frac{v_{j-1/2}}{m_{j-1/2}} \qquad _o \qquad (6)$$

momentum:
$$\frac{DUJ}{Dt} = \left[(P+Q)_{J-1/2} - (P+Q)_{J+1/2}\right] \frac{A_J^N}{1/2(m_{J-1/2} + m_{J+1/2})} \qquad (7)$$

energy:
$$E_{J-1/2}^{N+1} = E_{J-1/2}^{N} - \left[1/2(P_{J-1/2}^{N} + P_{J-1/2}^{N+1}) + Q_{J-1/2}^{N+1/2}\right]\left[V_{J-1/2}^{N+1} - V_{J-1/2}^{N}\right] \qquad (8)$$

state:
$$E_{J-1/2}^{N} = E(P_{J-1/2}^{N}, V_{J-1/2}^{N}) \qquad (9a)$$

for $2H_2 + O_2$ and air

$$P_{J-1/2}^{N} = P(E_{J-1/2}^{N}, V_{J-1/2}^{N}) \text{ for PETN} \qquad (9b)$$

artifical viscosity:
$$Q_{J-1/2}^{N+1/2} = C^1 \frac{(U_J^{N+1/2} - U_{J-1}^{N+1/2})^2}{V_{J-1/2} + V_{J-1/2}} \cdot \frac{\rho_o}{2} \qquad (10a)$$

for $U_J < U_{J-1}$

$$Q_{J-1/2}^{N+1/2} = O \qquad (10b)$$

for $U_J > U_{J-1}$

The quantity A^N, represents the area of a particular interface where DU/Dt is the acceleration of the interface. The constant C^1 in the artifical viscosity is related to the usual constant C, by the equation $C^1 = C^2/4$ (for further details see Ref 10).

A particular solution is obtained by integrating the momentum equation, Eq 2, twice, to get new velocities and positions for the next time step. From the new position a new specific volume is calculated for each zone and a simultaneous solution of the energy and state equations, Eqs 8 and 9, gives the new pressure and energy. A new time step is then calculated subject to the Courant and the artificial viscosity stability conditions[10], and the process is then repeated.

During the course of the analysis, several difficulties were found to exist near the origin, where there is a discontinuity in going from a spherical to a planar geometry. In reality, the flow around the origin cannot be considered as one-dimensional, as it is actually a radially-symmetric, two-dimensional phenomenon.

The use of the artificial viscosity technique may be strongly criticized when it is applied in the region surrounding the origin. In the spherical geometry this technique is valid only as long as the shock thickness is small compared with the radius of the shock, and this condition is clearly violated near the origin.

In addition, there are very severe zoning problems. The effect of a discontinuity on zone mass has been studied and it had been found that to obtain precise results, there should not be significant discontinuities in zone mass, particularly at the interface between the $2H_2+O_2$ mixture and the air. Consider the movement of the interface between the gas mixture $2H_2+O_2$ in the chamber and the air in the barrel, at the time when the diaphragm breaks. This movement is governed by the momentum equation, Eq (7),

$$\frac{dU_J}{dt} = \frac{A_J^N \left[(P + Q)_{J-1/2} - (P + Q)_{J+1/2} \right]}{1/2 \, (m_{J-1/2} + m_{J+1/2})}$$

For a given pressure difference across the interface, the acceleration depends on the values of the masses $m_{J-1/2}$ and $m_{J+1/2}$. But, due to the very low pressure in the barrel, $m_{J+1/2}$ is very small and is negligible compared with $m_{J-1/2}$, so that the acceleration of the interface is almost inversely proportional to the mass of the last zone in the chamber. However, the continuity in zone mass was impossible to maintain, since the density of the combined gas is very high (in some cases $\sim 1.0 \text{g/cm}^3$). It was therefore necessary to compromise, such that the formation of the planar shock in the channel was not instantaneous, and the final velocity was approached exponentially in a time that depended on the zone mass. That is, the dense mass zone behaves like a projectile. To improve the precision of the calculations, many more zones must be taken in the highly dense gas in order to have continuity in zone mass across the interface

of the gases $2H_2+O_2$-Air. But, if very fine zones are used, then the computing time becomes too costly.

A computed wave-speed diagram of the shock-tube case having a 5/16 in dia (8 mm) launcher barrel or shock tube channel appears on Fig 3. It is seen that for an 8 in dia (20.3 cm) hemispherical driving chamber with $2H_2+O_2$ at 200 psi (13.6 atm) initial, a shell of PETN weighing 200 g, and a counterpressure of air of 1.0 torr, produces a shock velocity of 32.8 km/sec, or a shock Mach number of 95. The above is by no means an optimum driving condition and stronger shocks could be produced with optimized higher explosive loading (beyond a maximum explosive charge, the shock strength will be decreased by wave interactions)(see also Ref 8)and initial conditions.

The wave diagram shows some other major features. The detonation wave in the $2H_2+O_2$ mixture is initiated instantly at the origin (t =0, x = 10 cm). It races at 2.9 km/sec to initiate the PETN liner when it strikes the surface and reflects as a shock to overtake the previous shock wave. A single imploding shock wave(as well as reflected rarefaction wave and a new contact surface, the details have been omitted on the diagram for simplicity throughout) is thereby generated. The imploding shock wave strikes the diaphragm (which is assumed to break instantly) at the origin station, producing a reflected hemispherical shock wave in the driving chamber and the primary planar shock wave followed by a contact surface in the channel. The process is repeated many times, as shown. However, the other shock waves that enter the channel are too slow to overtake the primary shock wave.

It is of interest to note that the computed results do not show any shock wave decay, and the computed pressure profiles (see Fig 4) show a uniform flow behind the planar shock wave. In practice there is a severe decay probably arising from blast wave effects (indicated by the motion reversals of the contact front between the explosive gases and the hydrogen-oxygen driver gas after 50μs), viscous losses, and ablative losses from the chamber and channel walls.

The wave motions and the pressure histories in the chamber and channel, as a function of time, are shown in Fig 4. The reflection of the rarefaction wave at the periphery of the chamber and the wave motions about the origin are clearly shown. The development of the primary shock wave with time is readily seen and an ideal uniform flow appears to develop. Nearly 200 cm of this hot gas is available at t = 407μ sec. However, as noted above this idealization is not achieved.

3. EXPERIMENTAL RESULTS

Some experimental work was done with the actual 8 in dia chamber. It was not meant to be an extensive study of the performance of this type of shock tube. Rather, it was aimed to check the results of the computations and to give an estimate of the losses, as the computer code did not take account of them. However, this preliminary work has been extremely helpful in assessing the deficiencies of the code and in the design of a new 25 mm dia shock tube that will not suffer from as many viscous effects.

The results were obtained in an 8 in dia chamber. The barrel was a stainless steel, high-pressure tube having a 5/16 in (8 mm) internal diameter. It was approximately 4 m long. A stainless-steel, scribed diaphragm 0.015 in (0.4 mm) thick, previously calibrated, was used to separate the channel from the hemispherical driver near the origin.

The velocities of the shocks were measured using three different methods. Five ionization probes were placed along the barrel 14 in (36 cm) apart to detect the arrival of the ionization front. These were corroborated by using small optical windows and photomultipliers to detect the luminous front at the same stations. The agreement was excellent. Additional substantiating velocity data for the 400 psi case, as shown on Fig 5, were obtained with a 34.4 Ghz (12 mm wave length) microwave Doppler system[12]. The agreement was again satisfactory.

A summary of the experimental results that have been obtained to date appears in Fig 5. It shows the maximum average velocities and their decay over a distance from 10 to 225 cm using 200, 400 and 600 psi $2H_2+O_2$ initial into 1.0 torr air, without explosive liners. It is seen that maximum average velocities of 5.3, 8.2 and 13.7 km/sec, respectively, are obtained near the origin giving shock Mach numbers of $M_s \sim$ 6, 24 and 40. The rate of decay of the shock is very high. For example, it drops from $M_s \sim$ 40 to $M_s \sim 11$, in a distance of about 180 cm, or an average Mach number decay rate of approximately $\Delta M_s/1 \sim 5/ft$. Such high rates of decay can be expected if we consider the very small diameter of the channel and the prevailing high shock Mach numbers and a detonation driver that relies on focussed implosions that can give rise to several loss mechanisms[13]. The present results are also in reasonable agreement with the recent work of Ref 14, on the Voitenko launcher.

4. CONCLUSIONS

Considerable additional work will have to be done in order to

evaluate the influence of radiative, convective, ablative and frictional losses; to optimize performance; to assess the future possibilities of this unique facility. Nevertheless, when one considers the sophisticated electrical condenser banks and switching equipment that is required even to produce $M_s \sim 40$ for electromagnetic drivers, this facility offers some worthwhile possibilities, especially with explosive liners when shock Mach numbers in the hundreds appear possible even with low density PETN ($\rho \sim 0.6$ g/cc) and very much greater with high-density PETN ($\rho \sim 1.5$ g/cc).

The existing facility will be used in the very near future to extend the present results by employing PETN with the $2H_2 + O_2$ driver into 8 mm and 25 mm channels with various gas counterpressures. Very much higher shock Mach numbers can be expected. At the same time, numerical analyses will be done to keep pace with and to guide the experimental program.

ACKNOWLEDGEMENTS

REFERENCES

1. Robert F. Flagg and I. I. Glass, "Explosive-Driven, Spherical Implosion Waves," The Physics of Fluids, Vol 11, No 10, pp 2282-2284, October 1968.

2. I. I. Glass, Shock and Combustion-Wave Dynamics in an Implosion-Driven Hypervelocity Launcher, UTIA Review No 25, 1965. (Also available as an AIAA preprint 25-108) .

3. Robert F. Flagg, The Application of Implosion Wave Dynamics to a Hypervelocity Launcher, ARL Report No 67-0220, Dec 1967 (also available as UTIAS Report No 125).

4. I. I. Glass, " Research Frontiers at Hypervelocities", CASI Jl Vol 13, No 8 and Vol 13, No 9, 1967, pp 348-366 and 401-426.

5. H. L. Brode, J. Appl. Phys. 26, 6 p 766 (1955).

6. H. L. Brode, Rand Corp. Memorandum RM-5187-PR, 1967.

7. J. Neumann and R. P. Richtmyer, J. Appl. Phys. 21, p 232 (1950)

8. P. A. L. Sevray, Performance Analysis of UTIAS Implosion-Driven Hypervelocity Launcher , UTIAS Technical Note No 121, January, 1968. (Also, ARL 68-0018, January 1968)

9. Robert F. Flagg and Gregory P. Mitchell, An Optimization Study of the UTIAS Implosion-Driven Hypervelocity Launcher Mk II, UTIAS Technical Note No. 130, 1968.

10. J. C. Poinssot, A Preliminary Investigation of a UTIAS Implosion-Driven Shock Tube, UTIAS Technical Note No 136, January, 1969.

11. A. Elsenaar, A numerical Model for a Combustion-Driven Spherical Implosion Wave , UTIAS Technical Note No 144, 1969.

12. A. Elsenaar, Microwave Measurements of Projectile Motion in the Barrel of the UTIAS Implosion Driven Hypervelocity Launcher , UTIAS Technical Note No 145, 1969.

13. D. E. Roberts, A Spectroscopic Investigation of Combustion-Driven Spherical Implosion Waves, UTIAS Technical Note No 140, May, 1969.

14. B. K. Crowley and H. D. Glenn, "Numerical Simulation of the Generation, Propagation and Attenuation of a High-Energy (Mach 120 to 40) Air-Shock Experiment", Proceedings, Seventh International Shock Tube Symposium, University of Toronto, 1970.

(A)

BARREL

CHAMBER

PROJECTILE
OR
DIAPHRAGM

EXPLOSIVE

$2H_2 + O_2$

(B)

(C)
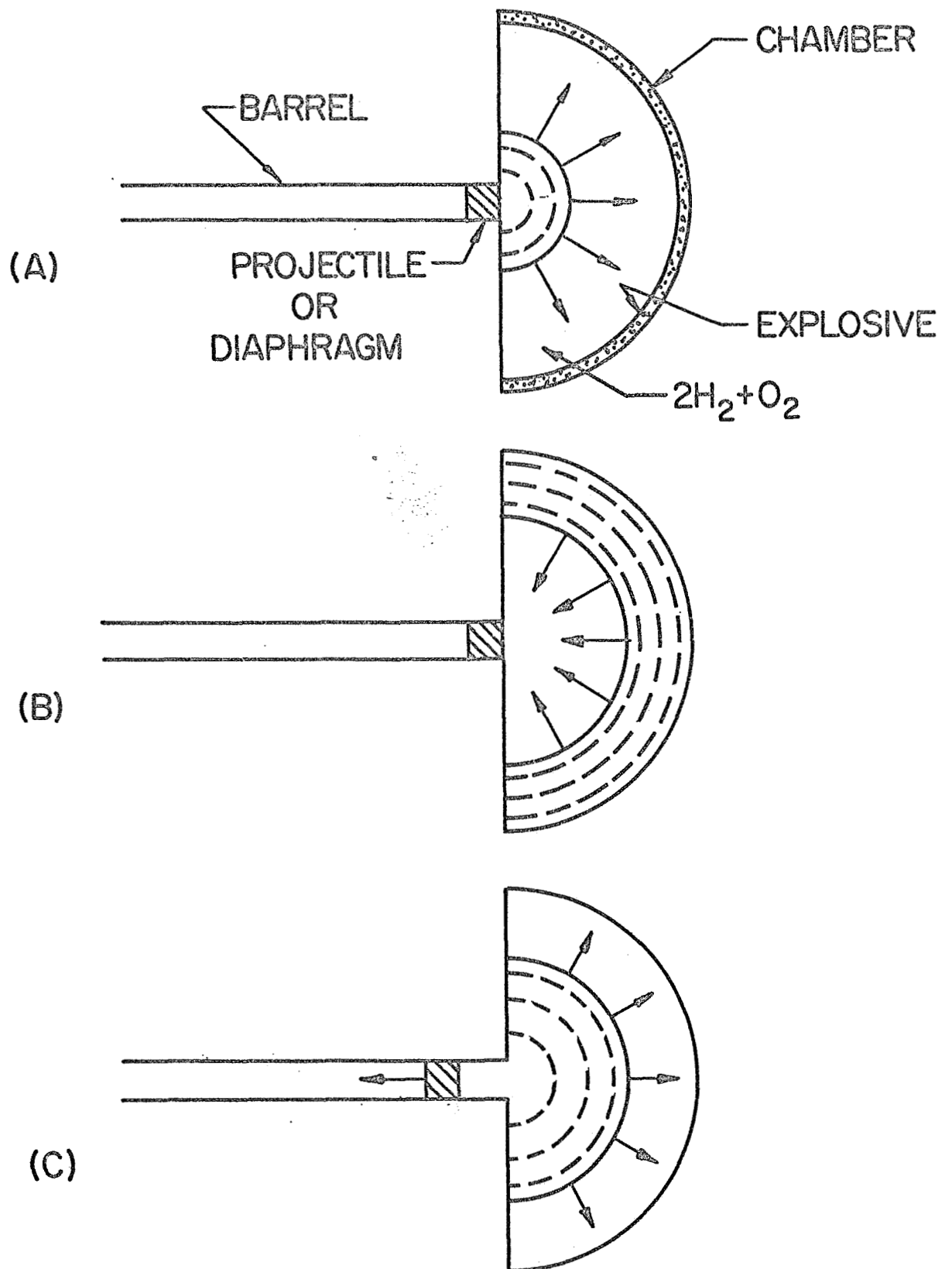
FIG. I   SCHEMATIC   OF   PRINCIPLE   OF   OPERATION
OF   UTIAS   HYPERVELOCITY   LAUNCHER
OR   SHOCK   TUBE
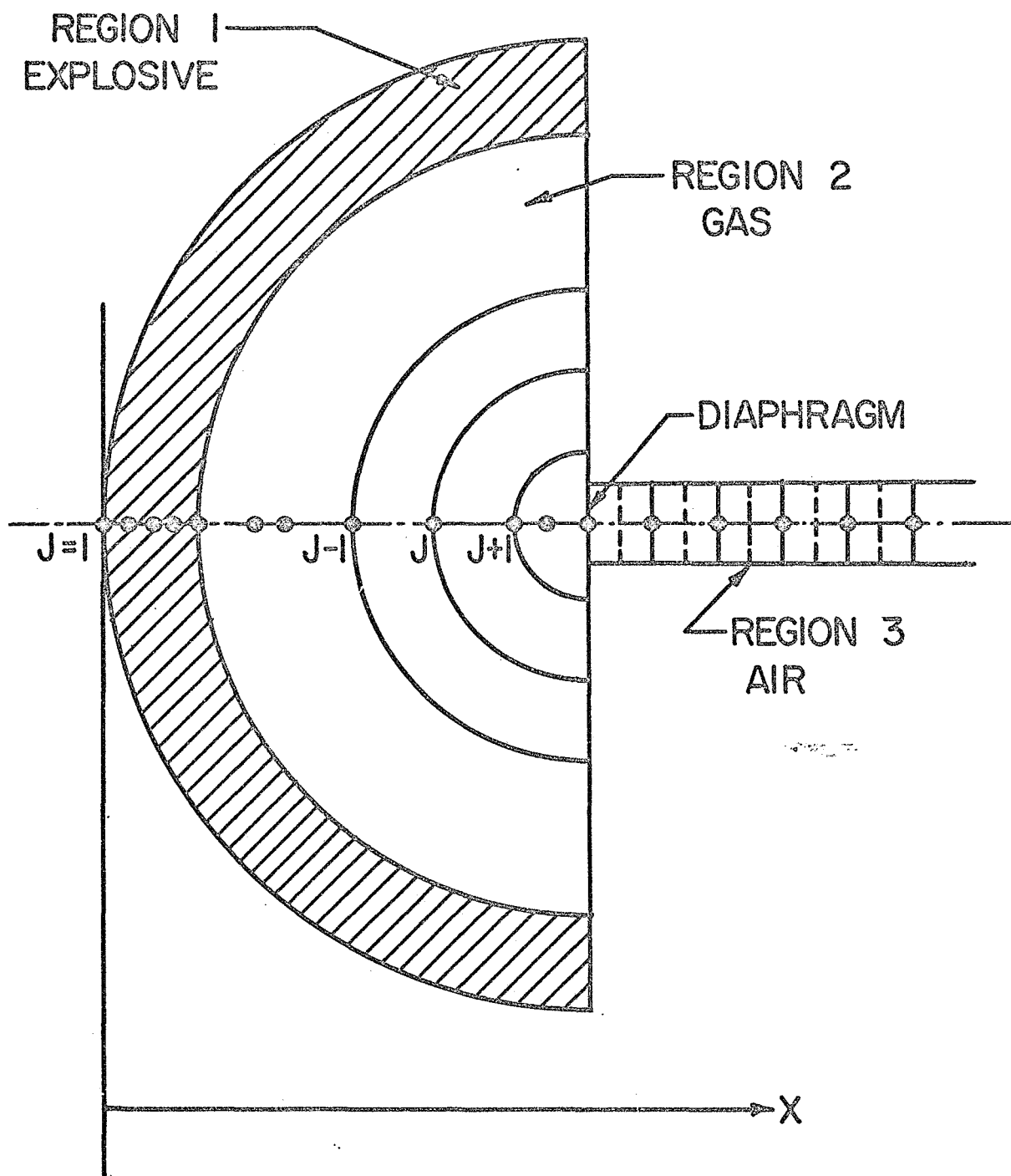
REGION 1
EXPLOSIVE

REGION 2
GAS

DIAPHRAGM

REGION 3
AIR

J=1   J-1   J   J+1

X

FIG. 2 DISTRIBUTION OF MASS POINTS

FIG. 3   WAVE-SPEED DIAGRAM IN THE (x,t)
PLANE FOR A UTIAS IMPLOSION-DRIVEN
SHOCK TUBE

FIG. 4   SHOCK TUBE CASE
PRESSURE PROFILES

200 PSI (13.6 ATM) 2H$_2$+O$_2$
200 g PETN
1 TORR COUNTERPRESSURE, AIR
8 IN (20 CM) DIA CHAMBER
5/16 (8MM) DIA BARREL

——— t = 107.65 μs
— — t = 206.50 μs
········· t = 306.92 μs
—·—·— t = 407.36 μs
   ⊙   INTERFACE

FIG. 5 EXPERIMENTAL SHOCK MACH NUMBER M_S VS. DISTANCE 8 IN (20.3 CM) DIA CHAMBER 5/16 IN (8MM) DIA BARREL; I TORR COUNTERPRESSURE, AIR; NO EXPLOSIVE